Journal of Colloid and Interface Science 522 (2018) 291–298

Contents lists available at ScienceDirect

Journal of Colloid and Interface Science

journal homepage: www.elsevier.com/locate/jcis

Regular Article

Binary gas mixture adsorption-induced deformation of microporous carbons by Monte Carlo simulation

Valeria Cornette [a,*], J.C. Alexandre de Oliveira [b], Víctor Yelpo [a], Diana Azevedo [b], Raúl H. López [a]

[a] Dpto. de Física, INFAP "Giorgio Zgrablich", Universidad Nacional de San Luis-CONICET, Ej. de los Andes 950, 5700 San Luis, Argentina
[b] Departamento de Engenharía Química, Universidade Federal do Ceará, Campus do PICI, Fortaleza, Brazil

GRAPHICAL ABSTRACT

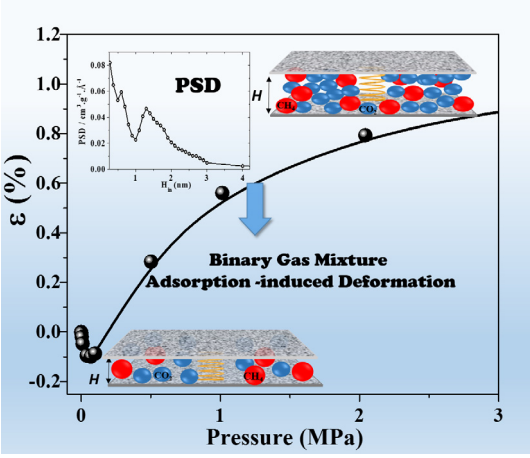

ARTICLE INFO

Article history:
Received 7 December 2017
Revised 19 February 2018
Accepted 10 March 2018
Available online 22 March 2018

Keywords:
Adsorption-induced deformation
Molecular simulations
Porous material

ABSTRACT

Considering the thermodynamic grand potential for more than one adsorbate in an isothermal system, we generalize the model of adsorption-induced deformation of microporous carbons developed by Kowalczyk et al. [1].

We report a comprehensive study of the effects of adsorption-induced deformation of carbonaceous amorphous porous materials due to adsorption of carbon dioxide, methane and their mixtures. The adsorption process is simulated by using the Grand Canonical Monte Carlo (GCMC) method and the calculations are then used to analyze experimental isotherms for the pure gases and mixtures with different molar fraction in the gas phase. The pore size distribution determined from an experimental isotherm is used for predicting the adsorption-induced deformation of both pure gases and their mixtures. The volumetric strain (ε) predictions from the GCMC method are compared against relevant experiments with good agreement found in the cases of pure gases.

1. Introduction

Gas adsorption in porous solids is known to induce elastic deformation, and this is well-documented in the literature, dating

* Corresponding author.
E-mail address: cornette@unsl.edu.ar (V. Cornette).

https://doi.org/10.1016/j.jcis.2018.03.026
0021-9797/

back to the first experimental evidence of swelling of charcoal by Meehan [2] and Bangham and co-workers [3] in the late 1920s. In microporous materials such as carbons and zeolites, the induced strain is usually very small (order of 10^{-3}) [4], and this effect has often been neglected in past discussions and modeling studies of adsorption experiments. However, this implies large internal stresses on the order of megapascals [5]. Although mechanical properties of microporous carbons are critically important for various technological applications, such as characterization of porous materials, equilibrium separation of fluid mixtures by porous sieves, and so on [6,7], the basic mechanisms of deformation during the adsorption-desorption processes are still not completely understood. Adsorption deformation is closely connected with the solvation pressure, which is a vast area of investigation due to its central role in adhesion, lubrication, pore swelling, adsorption at geological conditions, and colloid stability [8–11].

Deformation of an adsorbent during adsorption-desorption cycles depends on the internal structure of porous bodies. The slit model [7], which represents the material as a disordered collection of slit geometry pores of different sizes embedded in an amorphous matrix [12–17], is usually assumed for the characterization of activated carbons and has been extensively used in determining their Pore Size Distribution (PSD) [18–22]. The PSD is the primary characteristic of the porous solid because of its influence on adsorption, diffusion, and so on.

Kowalczyk et al. [1,23–25] in particular showed that the deformation effect caused by argon, carbon dioxide and methane adsorption in micropores may be highly sensitive to the micropore size distribution of the material under investigation and the kind of adsorbate applied. However, not many works have been devoted to the analysis of the solvation or disjoining pressure as applied to adsorption of a binary gas mixture. Recently, Brochard et al. [26] simulated the competitive adsorption of carbon dioxide and methane in CS1000 (a realistic model for microporous coal) and concluded that the competitive adsorption of the two fluids in the coal micropores is responsible for the differential swelling phenomenon, a major problem for field application of enhanced coal bed methane recovery (ECBM).

Furthermore, the adsorptive separation of gases is an important process in many industrial and environmental applications. In particular, the separation of CO_2 from CO_2-CH_4 mixtures is a fundamental problem in natural gas and biogas purification/upgrading in energy generation applications [27,28].

The aim of the present paper is to study the microscopic mechanism and calculate the adsorption-induced deformation of porous carbonaceous materials upon adsorption of carbon dioxide, methane and their mixtures. In order to achieve this purpose, we use and further explore (and generalize for mixtures) the model thermodynamic approach developed in Ref. [1] and employ Monte Carlo simulations to compute the adsorption stress in slit-shaped carbon pores of various sizes. Finally, we predict the adsorption-induced deformation for the activated carbon Norit R1 Extra sample, for three adsorptive concentrations of binary mixtures and discuss the results.

2. Theory: Thermodynamic methodology

We consider a pure fluid confined between a single slit-shaped pore separated by a distance H and in equilibrium with a reservoir of bulk fluid at temperature T and chemical potential μ. For a large separation H, the force per unit area exerted by the fluid on the walls is the pressure of the bulk fluid p (external pressure), but as H decreases and becomes of the order of the range of the intermolecular forces, the force per unit area, $\sigma_S(H, p)$ differs from the bulk fluid value. Solvation pressure, solvation force, or disjoining pressure because of fluid adsorption is the cause of elastic deformation of the adsorbent, which can be measured directly. The calculated solvation pressure may be either positive or negative, which causes either contraction or swelling, respectively. The solvation pressure p_s can be obtained by the following equation:

$$p_S(H,p) = \sigma_s(H,p) - p \tag{1}$$

The adsorption stress in a single slit-shaped pore of width H can be calculated from the grand thermodynamic potential as [8]:

$$\sigma_S(H,p) = -\frac{1}{A}\left(\frac{\partial \Omega_p}{\partial H}\right)_{T,p} \tag{2}$$

where A is the surface area, Ω_p is the grand free energy, H is the pore width and T is the temperature. Following previous studies [1], the volumetric strain measured in dilatometric experiments is given by

$$\varepsilon = \frac{\Delta V}{V} = \frac{\varphi}{k}\left[\bar{\sigma}_s - p\right] \tag{3}$$

In the above equation, the effective adsorption stress and bulk modulus are respectively expressed by

$$\bar{\sigma}_s = \frac{\int H\sigma_s(H,p)F(H)dH}{\int HF(H)dH} \tag{4}$$

$$K = \frac{k}{\varphi} \tag{5}$$

where φ is the porosity, k denotes the elastic modulus, which may depend on the pore width, $HF(H)\,dH$ is the differential pore size distribution which is commonly calculated from the adsorption isotherms.

In order to calculate the volumetric strain, one first has to compute the adsorption stress in individual pores and then to average this stress with the pore size distribution function. As we can see, the distribution is key to this problem.

2.1. Calculation of the solvation pressure and the volumetric strain

For the purpose of considering the effects of swelling and shrinkage, the next steps are followed:

(1) The adsorption stress in individual slit-shaped pores is calculated from Eq. (2). This method requires the thermodynamics integration along the simulated isotherm for each size pore H, which allows to compute the grand thermodynamic potential $\Omega_p(\mu, T)$ and, subsequently, the differentiation of $\Omega_p(\mu, T)$ with respect to H:

$$\Omega_p(\mu,T) = \Omega_0\left(\mu_r,T\right) - \int_{\mu_r}^{\mu} N d\mu \tag{6}$$

$$\sigma_s(p,H) = k_B T\left[\frac{\partial N(p^r)}{\partial H} + \frac{\partial}{\partial H}\int_{lnp^r}^{lnp} N d\ln p\right] \tag{7}$$

Here, $N(H, T, p)$ is the number of adsorbed molecules per surface area in the pore of width H at given environmental conditions, pressure p, temperature T and ideal gas as reference state (r). Considering the grand potential for more than one adsorbate in an isothermal system [29]:

$$d\Omega = -\sum_i N_i d\mu_i = -k_B T\sum_i \frac{N_i}{f_i} df_i \tag{8}$$

At constant grand potential and constant temperature, Eq. (8) reduces to the isothermal, isobaric Gibbs-Duhem:

$$\sum_i N_i d\mu_i = 0(constant, T, \Omega)$$

Therefore, under the restriction of constant grand potential, adsorbed solutions can be handled as ideal or non-ideal solutions using the same methods and equations developed for vapor-liquid equilibria. Assuming phase equilibrium, the chemical potentials of the adsorbed species are calculated from the specified temperature, pressure, and composition (Y) of the bulk gas phase using an appropriate equation of state. In this study, the chemical potential was calculated using the Peng-Robinson equation [30].

It is possible to generalize the Eq. (7) to more than one species as:

$$\sigma_s(p.H) = k_B T \sum_i \left[\frac{\partial N_i(f_i^r)}{\partial H} + \frac{\partial}{\partial H} \int_{lnf_i^r}^{lnf_i} N_i d\ln f_i \right] \quad (9)$$

where $f_i$is the fugacity of species i. Note that the fugacity coefficient depends on the molar fraction of the species in the mixture.

(2) The effective adsorption stress is calculated from Eq. (4). One has to average the adsorption stress σ_s(H, p) with a pore size distribution (PSD) function. In the present work, the PSD is obtained from a kernel of simulated isotherms of a pure gas. This method is explained below.
(3) Finally, the volumetric strain ε from Eq. (3) can be predicted, considering different values of elastic modulus and the PSD calculated in the previous step.

3. Molecular simulation

The adsorption isotherms were computed by the GCMC. The implementation of this simulation method is well established [31–33].

The interaction between adsorbate molecules is modeled using the truncated Lennard-Jones potential

$$U_{ff}(r) = -4\varepsilon_{ff}\left[\left(\frac{\sigma_{ff}}{r}\right)^6 - \left(\frac{\sigma_{ff}}{r}\right)^{12}\right] \quad (10)$$

where ε_{ff} and σ_{ff} are the energetic and geometrical parameters of the LJ potential and r is the molecular separation. Each wall of the model graphitic slit pore was represented by a series of stacked planes of LJ atoms. The interaction energy between a fluid particle and a single pore wall at a distance z (measured between the centers of the fluid atom and the atoms in the outer layer of the solid) was described by the Steele's 10-4-3 potential [33].

$$U_{gs-STEELE}(z) = 2\pi\,\varepsilon_{fs}\rho_C\,\sigma^2{}_{fs}\Delta\left\{\frac{2}{5}\left(\frac{\sigma_{fs}}{z}\right)^{10} + \left(\frac{\sigma_{fs}}{z}\right)^4 - \frac{\sigma^4{}_{fs}}{3\Delta(z+0.61\Delta)^3}\right\} \quad (11)$$

where Δ is the separation between layers in graphite (0.335 nm), ρ_c is the number density of carbon atoms per unit volume of graphite (114 nm^{-3}), ε_{fs} and σ_{fs} are the solid-fluid Lennard-Jones parameters. The cross LJ parameters are determined using the standard Lorentz-Berthelot combining rules (arithmetic mean for collision diameter and geometric mean for well depth). The values of the parameters included in the interaction potentials (Eqs. (9) and (10)) are given in Table 1 [34,35].

Four types of elementary steps are performed randomly in each attempt of the GCMC simulation [31,36] displacement, adsorption, desorption, and identity-swapping. Transition probabilities for each Monte Carlo attempt are given by the usual Metropolis rules.

Table 1
Parameters used in the LJ potentials for the GCMC simulations.

Molecule	σ_{ff} (nm)	ε_{ff}/k_B (K)	σ_{fs} (nm)	ε_{fs}/k_B (K)
CO_2	0.3615	241.7	0.3507	81.3
CH_4	0.3751	147.8	0.3575	64.3
N_2	0.3615	101.6	0.3507	56.3
Carbon	0.3400	28.0	–	–

Boltzman constant $k_B = 1.380/650424 \times 10^{-23}$ (J/K).

The use of identity-swapping (only for mixture) trials did not affect the GCMC averages; however, as it was expected [37,38], it improved convergence, considerably reducing the magnitude of standard deviations.

The lateral dimensions of the cell for the slit geometry were taken as L = 25 σ_{ff} and periodic boundary conditions were used in these directions. The cutoff distance, beyond which the potential is neglected, is set to be 5σ. Equilibrium was generally achieved after 10^8 MC attempts, after which mean values were taken over the following 10^8 MC attempts for configurations spaced by 10^3 MC attempts, in order to ensure statistical independence.

The accessible pore volume could be defined in a way such that the center of the molecule should be available in the volume space where the solid-fluid potential is negative. Thus, if we let z_0 be the distance at which the solid-fluid potential is zero, we will take the accessible width for adsorbate molecule as:

$$H' = H_{cc} - 2z_0 + s \quad (12)$$

Here, H_{cc} is the physical width of the pore, which is defined as the distance from the plane passing through all carbon atoms of the outermost layer of one wall to the corresponding plane of the opposite wall. This formula was first suggested by Everett and Powl [39], and later by Kaneko et al. [40]. In this way, the adsorption excess (and therefore the adsorption isotherm), as well as other thermodynamic quantities of interest, like the isosteric enthalpy of adsorption, can be calculated.

4. Calculating the pore-size distribution

Davies et al. [19] and Davies and Seaton [41,42] have addressed in detail the problem of calculating PSDs from adsorption data. Therefore, we present here only the most important aspects of the solution procedure.

The theoretical overall adsorption isotherm (θ^{theor}) can be expressed as a superposition of isotherms corresponding to each pore size (H_j), pressure P and temperature T, called local isotherms, θ_L, each one with a weight corresponding to the pore size distribution, $f(H_j)$:

$$\theta_i^{theor} = \sum_{j=1}^{m} \theta_L(H_j^*, P_i, T)\, f(H_j^*)\, \delta H_j^* \quad (13)$$

where m is the number of quadrature intervals used in the analysis, and H^* is the midpoint of each quadrature interval. Eq. (4) cannot be solved directly due to the ill-posed and ill-conditioned properties of these equations. The detrimental effect of both of these properties can, however, be minimized by employing regularization. The PSD is then obtained by fitting Eq. (4) plus the regularization term, as proposed by (Davies et al. [19]; Davies and Seaton [18]), numerically via a fast non-negative least square algorithm. This is the most commonly used method to stabilize the result, incorporating additional constraints that are based on the smoothness of the PSD (Wilson [43]; Szombathely et al. [44]; Merz [45]; Whaba [46]; Hansen [47]). Physically, this method corresponds to recognizing that a real PSD is more likely to be relatively smooth and centered around a few dominant pore sizes rather than highly fragmented and spiky. One complicating factor in employing regularization is that it requires

the identification of an optimal smoothing parameter to be used in the analysis; we have used L curves to determine the optimal amount of smoothing. L curves (Jagiello [48]) are a plot of some measure of the error of the fit to the data against the smoothing parameter. In general, the error of the fit to the data increases as the value of the smoothing parameter increases. However, below a threshold value of the smoothing parameter, the increase in the error is often negligible, while above the threshold the error increases rapidly. Plots of the error against the smoothing parameter, therefore, resemble an "L" lying on its side. These curves are used to identify this threshold value, which is taken to be the optimal extent of smoothing. PSD solutions satisfying minimum L-curve and the generalized cross-validation criteria have been shown to have superior predictive performance compared to other possible PSD solutions (Davies et al. [19], Davies and Seaton [41] and Pinto Da Costa [49]).

Pore size distributions for slit pores have been calculated with kernels containing 51 pore sizes between 0.28 and 7 nm and 31 relative pressure points ($2.8 \times 10^{-4} - 4.3$ MPa) for CO_2, and 53 pore sizes between 0.28 and 7 nm for CH_4 and 17 relative pressure points ($2.8 \times 10^{-3} - 5.7$ MPa). Gusev et al. [50] recognized that for a given set of data, there is a maximum pore size that can be identified reliably in a PSD analysis. Differentiating large pores from one another is difficult because the extent of adsorption is virtually indistinguishable from one pore to another. This difficulty arises when the adsorption onto the opposite walls of a single pore occurs essentially independently (that is, the pore walls become too far away from each other to enhance adsorption). The pore size above where this occurs depends on the adsorptive and it is a function of the temperature and the pressure. Gusev et al. [50] therefore introduced the concept of a "window of reliability" (WR) into PSD analyses. This "window" extends from the smallest pore that the adsorptive can enter to the largest pore that can be reliably distinguished from the next largest pore. Since the adsorption in all the pores larger than those in the window of reliability is essentially indistinguishable, assigning a single quadrature interval to this region makes a better use of the experimental data [19].

5. Results and discussion

5.1. Adsorption isotherms of pure gases, PSDs and solvation pressure in individual pores

Adsorption-induced deformation of activated carbons can be easily predicted from an assumed pore size distribution and bulk modulus. Unlike previous studies where the pore size distribution (PSD) was modeled by the Gaussian functions [1,24], in the current paper, the PSD is derived by means of solution of the integral adsorption equation, which presents the experimental isotherm (N2 at 77 K) as the convolution of the kernel of simulated isotherms.

In other words, we propose, as a starting point, a PSD obtained on the assumption that the solid is rigid (nondeformable). Under normal adsorption conditions (low pressure), a rigid pore model should be a good approximation to the deformable model investigated here [51].

Fig. 1 presents the PSDs calculated from the collection of N_2 simulated isotherms at 77 K using our own GCMC, and using NLDFT (Quantachrome's data reduction software) and the corresponding theoretical fit. The experimental data were obtained by Dreisbach et al. [52] on activated carbon Norit R1 Extra. As a first examination, it can be observed (inset in Fig. 1) that the PSDs obtained fit satisfactorily the experimental isotherm. This result indicates that the PSD obtained by GCMC simulations represents properly the considered activated carbon. Therefore, in this work, we propose to use this PSD (GCMC) to predict the volumetric strain for both pure gases (CO_2 and CH_4) and mixtures.

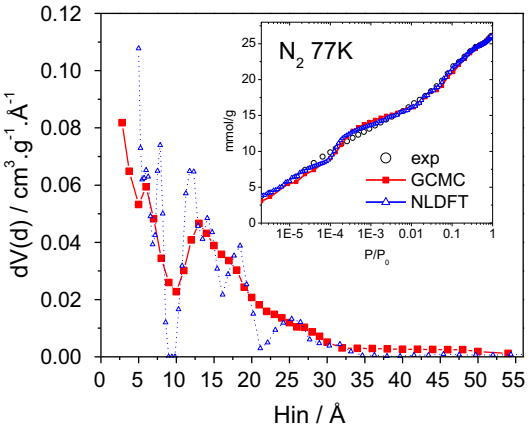

Fig. 1. Pore size distribution using GCMC simulation and NLDFT methods. Inset: N_2 (77 K) adsorption isotherm on activated carbon Norit R1 Extra, experimental data, GCMC and NLDFT fit.

The resulting PSD (NLDFT) shows a gap of pores around 10 Å. This feature is supposed to be an artifact introduced by the perfect graphene sheets modeling assumptions. This problem could be fixed with the QSDFT method [53]. It is important to keep in mind that the PSD was obtained using the independent pore models (Eq. (13), therefore the deformation in a solid would depend on the connectivity of its pores.

The variation of adsorption stress versus slit-shaped carbon pore size and versus the external bulk pressure is shown in Fig. 2 for both pure gases (CO_2 and CH_4). The characteristic nonmonotonic dependence of the adsorption stress on the pore size in the range of micropores is found.

It has been proposed by several authors [8] that the maxima in the adsorption stress correspond to "ordered" states, where the molecules are efficiently arranged in layers, and the available space is utilized in the best way. The computed adsorption stress is high in the smallest pores because of high adsorption and compression of adsorbed gas molecules. For example, in the CO_2 case (Fig. 3a), the solvation pressure in a 2.9 Å micropore reaches 1800 MPa. As pore size reaches 3.7 Å for CO_2 and 3.9 Å for CH_4, the solvation force crosses zero and it is further negative. Further expansion of the pore size results in a fast reduction of the solvation force.

The volumetric strain was calculated from Eq. (3) for pure gases using the differential PSD-GCMC previously obtained (Fig. 1). The corresponding CO_2 and CH_4 induced deformation curves at 298 K are shown in Fig. 3. The observed behavior can be understood considering the molecular size and the interaction energy of each species, which is regarded by the potential parameters (σ_{gs}/σ_{gg}, $\varepsilon_{gs}/\varepsilon_{gg}$) [8]. This ratio plays a crucial role in the balance between the attractive and the repulsive interactions. The effect of molecular size on salvation pressure (and therefore in strain volumetric) is to cause a phase shift and also a change in amplitude of the oscillations while interaction energy only affects oscillations amplitude.

On the one hand, the CO_2 molecule is smaller than CH_4 with stronger binding energy, therefore, the smallest pores size, which presents only expansion, will be mainly involved in the adsorption-induced deformation process. On the other hand, it can be noticed that adsorbed CH_4 induces lower deformation of porous carbon than CO_2, as well an initial contraction and further expansion.

The strain volumetric can be calculated to describe experimental data. The deformation curves obtained from differential PSD consider an appropriate value of elastic modulus (7 GPa and 15 GPa), which are compared to experimental dilatometric curves obtained by Yakovlev et al. [54] and Kowalzcyk et al. [24] to CO_2 and CH_4 adsorption respectively (Fig. 4). The bulk modulus value

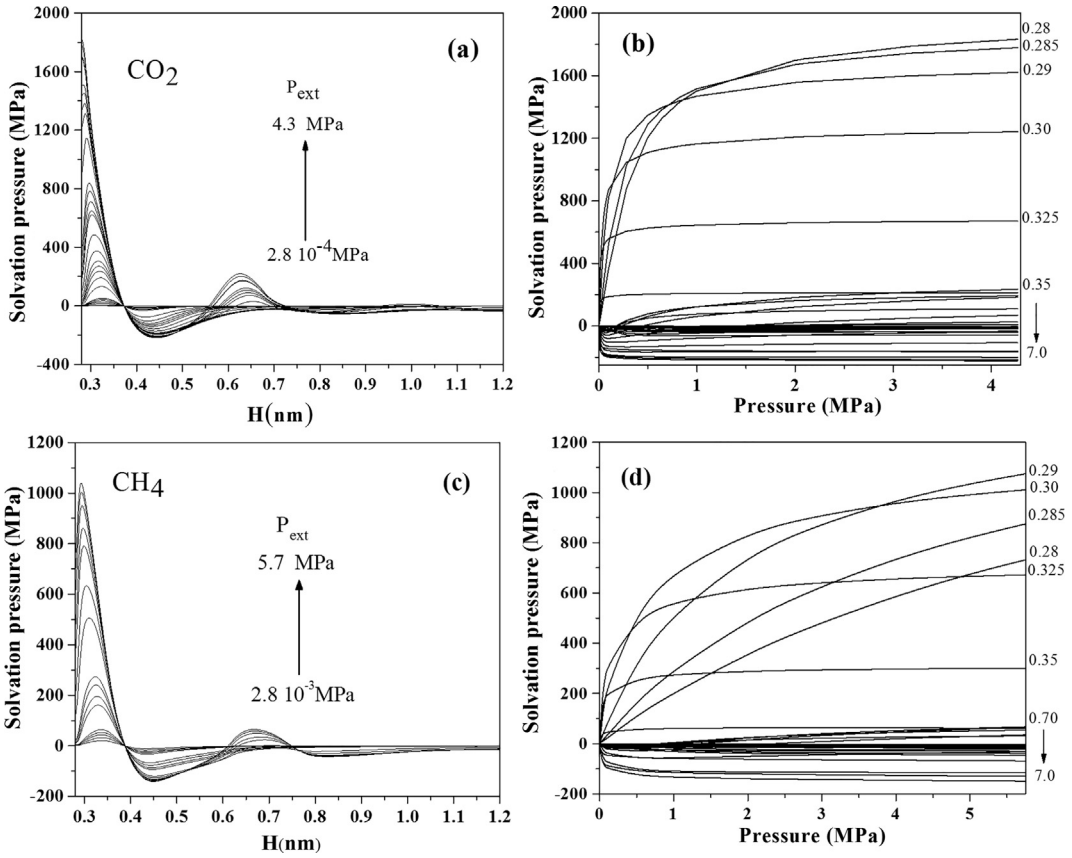

Fig. 2. Adsorption stress of (a) CO_2 and (c) CH_4 at 298 K versus slit-shaped carbon pore size. Adsorption stress of (b) CO_2 and (d) CH_4 versus external pressure for selected slit-shaped carbon pore sizes. Note that the size of the pore is displayed on the plot in (nm). Note the high solvation pressures in the smallest ultramicropores of pore width lower 0.35 nm.

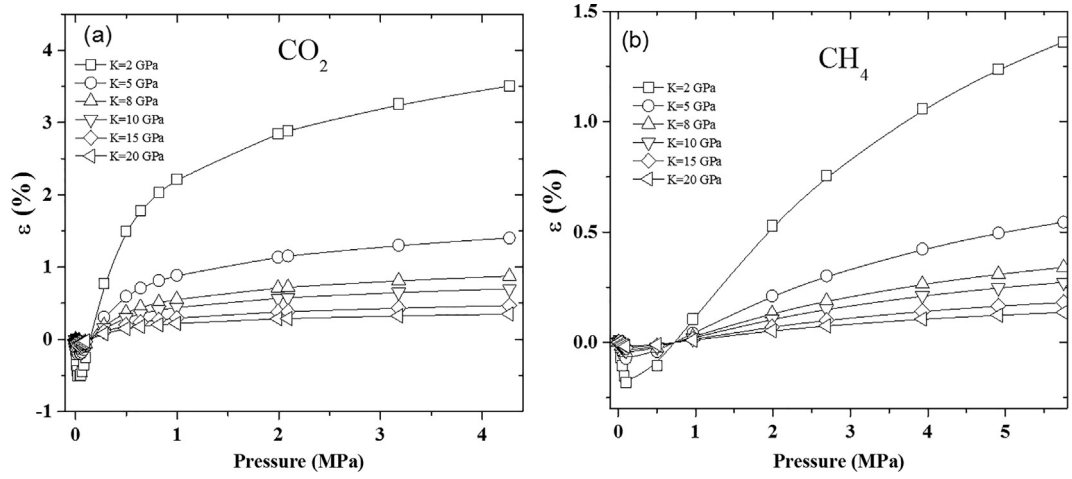

Fig. 3. Strain volumetric computed on the basis of pore volume distributions. The assumed elastic modulus *K* is indicated in plots.

to carbide-derived activated carbon was reported in previous works as 7 GPa [1]. Despite considering different activated carbon and different temperatures, the predicted behavior of strain volumetric agrees with the experimental data.

5.2. Binaries mixtures.

Adsorption isotherms were simulated for CO_2-CH_4 binaries mixture considering three different molar fractions: Y_{CO2} = 0.78, Y_{CO2} = 0.46 and Y_{CO2} = 0.046. The strain volumetric to mixture gases can be predicted from Eq. (8) using the kernels of simulated pure CO_2 and CH_4 local isotherms, and the PSD shown in Fig. 1. The adsorption stress versus slit-shaped carbon pore size to three molar compositions is shown in Fig. 5.

As it was mentioned above, the adsorption stress or salvation pressure curves depend on the relation of potential parameters (σ_{gs}/σ_{gg}, $\varepsilon_{gs}/\varepsilon_{gg}$) for both gases and the molar fraction of each other in the mixture. In Fig. 6a, it is shown the adsorption stress curves corresponding to the fraction molar with more CO_2, and a similar behavior to pure CO_2 gas can be observed (Fig. 2a), due to

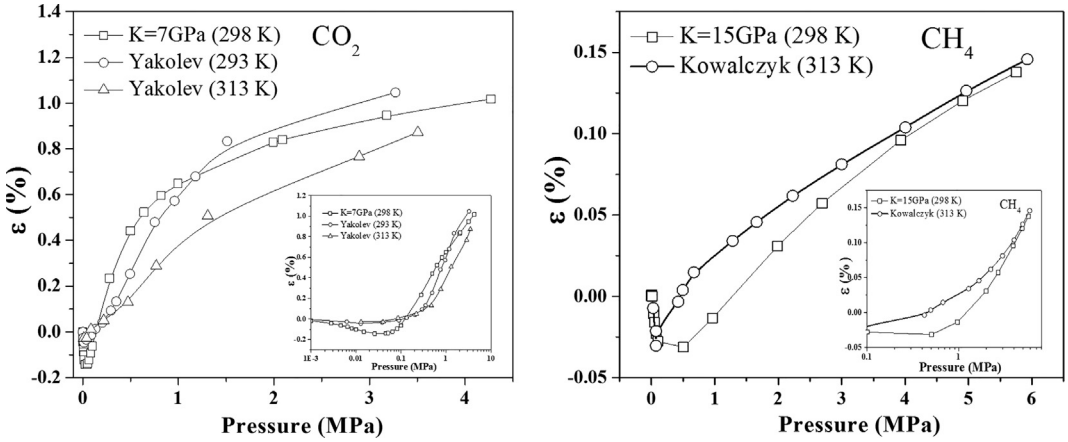

Fig. 4. Dependence of the deformation of activated carbon on the CO_2 adsorption at 313 K and 293 K and CH_4 at 313 K measured by the dilatometric method [24,54] and compared with the strain computed from the thermodynamic model.

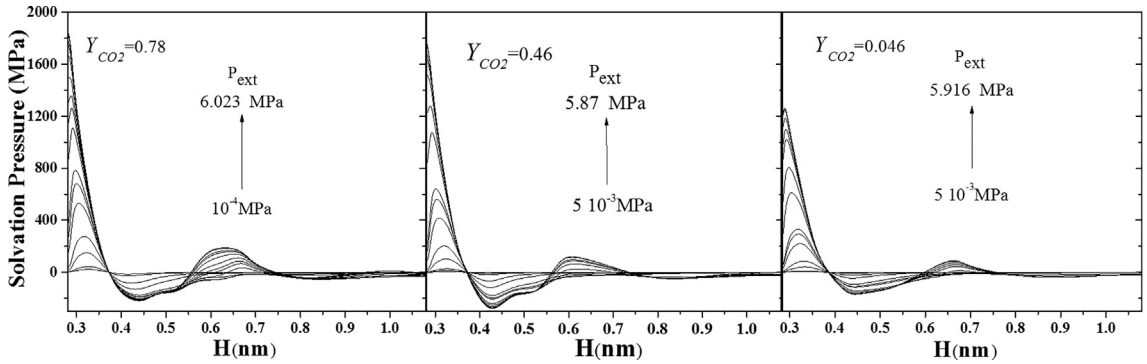

Fig. 5. Adsorption stress for the binary mixtures at 298 K versus slit-shaped carbon pore size.

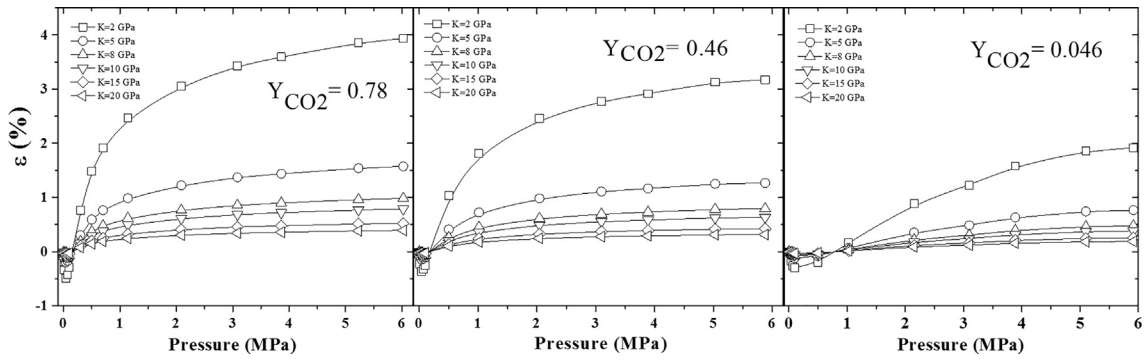

Fig. 6. Predicted adsorption-induced deformation curves for the different binary mixtures at 298 K computed on the basis of pore volume distribution displayed in Fig. 1.

this mixture containing a smaller CH_4 molar fraction. When a molar composition approximately equal is considered (Fig. 5b), the competition between two gases determines the behavior of adsorption stress curves. Therefore, because of CO_2 molecule is smaller than CH_4 with stronger binding energy, it can be expected that carbon dioxide is preferentially adsorbed to methane. Moreover, in Fig. 5c a molar fraction, where the CO_2 concentration is very low, is presented and, as expected, the adsorption stress curves are similar to CH_4 pure gas (Fig. 2c).

Finally, we can predict the strain volumetric for the three different concentrations presented in this work, from Eq. (3) by using the differential PSD previously calculated and tested (Fig. 1), and considering various elastic modulus values.

In Fig. 6(a)–(c), it can be observed the predicted adsorption-induced deformation for binary mixture CO_2–CH_4 at a different concentration, which is computed on the basis of pore volume distribution obtained for the activated carbon Norit R1 Extra (Fig. 1). A similar behavior is found for both molar fractions $Y_{CO2} = 0.78$ and $Y_{CO2} = 0.46$, and furthermore, this behavior is found for the pure CO_2 gas (Fig. 3a). The strain volumetric curves for the last molar fraction, as expected, show a similar behavior to pure CH_4 gas.

These observations are clearly shown in Fig. 7, where our results (set at K = 7 GPa) were confronted against both the experimental data and GCMC simulations of pure gases. Note that the adsorption of fraction molar near to pure gases ($Y_{CO2} = 0.78$ and

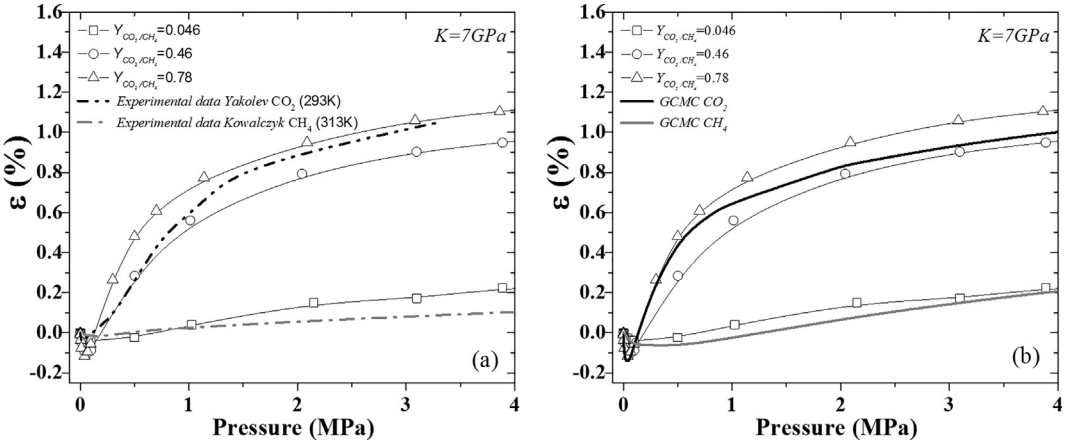

Fig. 7. Predicted adsorption-induced deformation curves of binary mixture at 298 K and $K = 7$ GPa computed from the thermodynamic method to three different molar fractions. The results are compared with pure species from (a) Experimental Data and (b) GCMC simulations from Kowalczyk's method.

$Y_{CO2} = 0.046$) induces greater adsorption stress than CO_2 and CH_4 pure adsorption respectively.

6. Conclusions

The main result of this work is to study and determine adsorption-induced deformation of pure components and binary mixtures of methane and carbon dioxide at 298 K in a specific activated carbon Norit R1 Extra [52] by GCMC simulation and thermodynamic model used in a previous study [1].

The shape of deformation curve strongly depends on the internal pore structure of porous body; consequently, the differential PSD that what chosen to obtain the strain volumetric from Eq. (3) is crucial to predict the deformation correctly. In this study, we propose to obtain the differential PSD from N2 experimental isotherm at 77 K. In Fig. 1, it was shown that the differential PSD calculated from experimental and simulated isotherms reproduces the experimental data and therefore, it is adequate to predict the adsorption-induced deformation of both pure gases and binary mixture in this kind of system.

Our calculations reproduce qualitatively the CO_2 and CH_4 stress-strain isotherms on activated carbon whose data were experimentally reported by Yakovlev et al. and Neimark et al. (Fig. 4). The elastic modulus value used to adjust experimental data were 7 GPa and 15 GPa. respectively, which are comparable with the reported data for vitreous carbons and polycrystalline graphite [1].

From the thermodynamic model of adsorption- induced deformation generalized to more than one species and knowing the pore size distribution of the investigated porous carbon, we can predict the strain volumetric of the thermodynamic model of adsorption-induced deformation not only for pure gases but also for binary mixture CO_2-CH_4. The results obtained can be useful for the interpretation of coal swelling/contraction upon adsorption of both carbon dioxide and methane.

Acknowledgements

The authors acknowledge financial support from CONICET (Argentina), CNPq (Brasil). The numerical works were done using the BACO parallel cluster (composed by 60 CPUs each with a Core 2 Quad processor and 50 CPUs each with an i7 processor) located at Dpto. de Física – Instituto de Física Aplicada, Universidad Nacional de San Luis – CONICET, San Luis, Argentina.

References

[1] P. Kowalczyk, A. Ciach, A.V. Neimark, Adsorption-induced deformation of microporous carbons: pore size distribution effect, Langmuir 24 (13) (2008) 6603–6608.
[2] F.T. Meehan, The expansion of charcoal on sorption of carbon dioxide, Proc. R. Soc. A Math. Phys. Eng. Sci. 115 (770) (Jun. 1927) 199–207.
[3] D.H. Bangham, N. Fakhoury, The expansion of charcoal accompanying sorption of gases and vapours [2], Nature 122 (3079) (1928) 681–682.
[4] V.Y. Yakovlev, A.A. Fomkin, A.V. Tvardovski, Adsorption and deformation phenomena at interaction of N2 and microporous carbon adsorbent, J. Colloid Interf. Sci. 280 (2) (Dec. 2004) 305–308.
[5] M. Colligan, P.M. Forster, A.K. Cheetham, Y. Lee, T. Vogt, J.A. Hriljac, Synchrotron X-ray powder diffraction and computational investigation of purely siliceous zeolite Y under pressure, J. Am. Chem. Soc. 126 (38) (2004) 12015–12022.
[6] S.J. Gregg, K.S.W. Sing, Adsorption, Surface Area and Porosity, second ed., Academic Press, 1982.
[7] H. Mash, F. Rodríguez-Reinoso, Activated Carbon, Elsevier Ltd, Oxford, 2006.
[8] P.B. Balbuena, D. Berry, K.E. Gubbins, Solvation pressures for simple fluids in micropores, J. Phys. Chem. 97 (4) (Jan. 1993) 937–943.
[9] S. Bakhshian, M. Sahimi, Adsorption-induced swelling of porous media, Int. J. Greenh. Gas Control 57 (2017) 1–13.
[10] K. Yang, X. Lu, Y. Lin, A.V. Neimark, Deformation of coal induced by methane adsorption at geological conditions, Energy Fuels 24 (11) (Nov. 2010) 5955–5964.
[11] K. Yang, X. Lu, L. Yangzheng, A.V. Neimark, Effects of CO_2 adsorption on coal deformation during geological sequestration, J. Geophys. Res. 116 (2011) 1–11.
[12] D. Nemirovsky, R. Moreh, K. Kaneko, T. Ohba, J. Mayers, Kinetic energy of neon atoms adsorbed on activated carbon, Surf. Sci. 526 (3) (2003) 282–290.
[13] K. Kaneko, C. Ishii, M. Ruike, H. Kuwabara, Origin of superhigh surface area and microcrystalline graphitic structures of activated carbons, Carbon N. Y. 30 (7) (1992) 1075–1088.
[14] C. Nguyen, D.D. Do, New method for the characterization of porous materials, Langmuir 15 (10) (1999) 3608–3615.
[15] M. Heuchel, M. Jaroniec, Use of simulated adsorption isotherms to study surface and structural heterogeneities of microporous solids, Langmuir 11 (11) (1995) 4532–4538.
[16] K.L. Murray, N.A. Seaton, M.A. Day, Analysis of the spatial variation of the pore network coordination number of porous solids using nitrogen sorption measurements, Langmuir 14 (17) (1998) 4953–4954.
[17] M. Heuchel, G.M. Davies, E. Buss, N.A. Seaton, Adsorption of carbon dioxide and methane and their mixtures on an activated carbon: simulation and experiment, Langmuir 15 (25) (1999) 8695–8705.
[18] G.M. Davies, N.A. Seaton, The effect of the choice of pore model on the characterization of the internal structure of microporous carbons using pore size distributions, Carbon N. Y. 36 (10) (1998) 1473–1490.
[19] G.M. Davies, N.A. Seaton, V.S. Vassiliadis, Calculation of pore size distributions of activated carbons from adsorption isotherms, Langmuir 15 (23) (1999) 8235–8245.
[20] J.P. Toso, V. Cornette, V.A. Yelpo, J.C.A. de Oliveira, D.C.S. Azevedo, R.H. López, Why the pore geometry model could affect the uniqueness of the PSD in AC characterization, Adsorption 22 (2) (2016) 215–222.
[21] C. Balzer, R.T. Cimino, G.Y. Gor, A.V. Neimark, G. Reichenauer, Deformation of microporous carbons during N_2, Ar, and CO_2 adsorption: insight from the density functional theory, Langmuir 32 (32) (2016) 8265–8274.
[22] P. Kowalczyk, C. Balzer, G. Reichenauer, A.P. Terzyk, P.A. Gauden, A.V. Neimark, Using in-situ adsorption dilatometry for assessment of micropore size distribution in monolithic carbons, Carbon N. Y. 103 (2016) 263–272.

[23] P. Kowalczyk, S. Furmaniak, P.A. Gauden, A.P. Terzyk, Carbon dioxide adsorption-induced deformation of microporous carbons, J. Phys. Chem. C 114 (11) (Mar. 2010) 5126–5133.
[24] P. Kowalczyk, S. Furmaniak, P.A. Gauden, A.P. Terzyk, Methane-induced deformation of porous carbons: from normal to high-pressure operating conditions, J. Phys. Chem. C 116 (2) (2012) 1740–1747.
[25] P. Kowalczyk, A. Ciach, A.P. Terzyk, P.A. Gauden, S. Furmaniak, Effects of critical fluctuations on adsorption-induced deformation of microporous carbons, J. Phys. Chem. C 119 (11) (2015) 6111–6120.
[26] L. Brochard, M. Vandamme, R.J.-M. Pellenq, T. Fen-Chong, Adsorption-induced deformation of microporous materials: coal swelling induced by CO_2-CH_4 competitive adsorption, Langmuir 28 (5) (Feb. 2012) 2659–2670.
[27] R. Babarao, Z. Hu, J. Jiang, S. Chempath, S.I. Sandler, Storage and separation of CO_2 and CH_4 in silicalite, C168 schwarzite, and IRMOF-1: a comparative study from Monte Carlo simulation, Langmuir 23 (2) (2007) 659–666.
[28] Y.-S. Bae et al., Separation of CO_2 from CH_4 using mixed-ligand metal-organic frameworks, Langmuir 24 (16) (2008) 8592–8598.
[29] A.L. Myers, P.A. Monson, Adsorption in porous materials at high pressure: theory and experiment, Langmuir 18 (26) (Dec. 2002) 10261–10273.
[30] J.M. Smith, H.C. Van Ness, M.M. Abbott, Introduction to Chemical Engineering Thermodynamics, New York, 1996.
[31] D. Frenkel, D. Smit, Understanding Molecular Simulation, Academic Press, Sidney, 1991.
[32] D. Nicholson, N.G. Parsonage, Computer Simulation and the Statistical Mechanics of Adsorption, Academic Press, London, 1982.
[33] W.A. Steele, The Interaction of Gases with Solid Surfaces, Oxford, 1974.
[34] D. Cao, J. Wu, Modeling the selectivity of activated carbons for efficient separation of hydrogen and carbon dioxide, Carbon N. Y. 43 (7) (2005) 1364–1370.
[35] P.I. Ravikovitch, A. Vishnyakov, R. Russo, A.V. Neimark, Unified approach to pore size characterization of microporous carbonaceous materials from N_2, Ar, and CO_2 adsorption isotherms, Langmuir 16 (5) (2000) 2311–2320.
[36] M.P. Allen, D.J. Tildesley, Computer Simulation of Liquids, Oxford University Press, Oxford, 1987.
[37] R.F. Cracknell, D. Nicholson, N. Quirke, A grand canonical Monte Carlo study of Lennard-Jones mixtures in slit shaped pores, Mol. Phys. 80 (4) (Nov. 1993) 885–897.
[38] Z. Tan, K.E. Gubbins, Selective adsorption of simple mixtures in slit pores: a model of Methane-Ethane mixtures in carbon, J. Phys. Chem. 96 (2) (1992) 845–854.
[39] D.H. Everett, J.C. Powl, Adsorption in slit-like and cylindrical micropores in the Henry's law region. A model for the microporosity of carbons, J. Chem. Soc. Faraday Trans. 1 Phys. Chem. Condens. Phases 72 (1976) 619–636.
[40] K. Kaneko, R.F. Cracknell, D. Nicholson, Nitrogen adsorption in slit pores at ambient temperatures: comparison of simulation and experiment, Langmuir 10 (12) (Dec. 1994) 4606–4609.
[41] G.M. Davies, N.A. Seaton, Development and validation of pore structure models for adsorption in activated carbons, Langmuir 15 (19) (1999) 6263–6276.
[42] G.M. Davies, N.A. Seaton, Predicting adsorption equilibrium using molecular simulation, AIChE J. 46 (9) (Sep. 2000) 1753–1768.
[43] J.D. Wilson, Statistical approach to the solution of first-kind integral equations arising in the study of materials and their properties, J. Mater. Sci. 27 (14) (1992) 3911–3924.
[44] M.V. Szombathely, P. Brauer, M. Jaroniec, The solution of adsorption integral equations by means of the regularization method, J. Comput. Chem. 13 (1992) 17–32.
[45] P.H. Merz, Determination of adsorption energy distribution by regularization and a characterization of certain adsorption isotherms, J. Comput. Phys. 38 (1980) 64–85.
[46] G. Wahba, Practical approximate solutions to linear operator equations when the data are noisy, SIAM J. Numer. Anal. 14 (4) (1977) 651–667.
[47] P.C. Hansen, SIAM Rev, vol. 24, no. 4, 1992, p. 561.
[48] J. Jagiello, Stable numerical solution of the adsorption integral equation using splines, Langmuir 10 (16) (1994) 2778–2785.
[49] J.M.C. Pinto da Costa, R.F. Cracknell, L. Sarkisov, N.A. Seaton, Structural characterization of carbonaceous combustion-chamber deposits, Carbon N. Y. 47 (14) (Nov. 2009) 3322–3331.
[50] V.Y. Gusev, J.A. O'Brien, N.A. Seaton, A self-consistent method for characterization of activated carbons using supercritical adsorption and grand canonical Monte Carlo simulations, Langmuir 13 (10) (1997) 2815–2821.
[51] D.D. Do, D. Nicholson, H.D. Do, Effects of adsorbent deformation on the adsorption of gases in slitlike graphitic pores: a computer simulation study, J. Phys. Chem. C 112 (36) (Sep. 2008) 14075–14089.
[52] F. Dreisbach, R. Staudt, J.U. Keller, High pressure adsorption data of methane, nitrogen, carbon dioxide and their binary and ternary mixtures on activated carbon, Adsorption 5 (3) (1999) 215–227.
[53] J.C.A. De Oliveira et al., On the influence of heterogeneity of graphene sheets in the determination of the pore size distribution of activated carbons, Adsorption 17 (5) (2011).
[54] V.Y. Yakovlev, A.A. Fomkin, A.V. Tvardovskii, V.A. Sinitsyn, Carbon dioxide adsorption on the microporous ACC carbon adsorbent, Russ. Chem. Bull. 54 (6) (2005) 1373–1377.